

Glueball masses in 4d U(1) lattice gauge theory using the multi-level algorithm

Pushan Majumdar*, Yoshiaki Koma[†], Miho Koma[‡]

Max-Planck-Institut für Physik, Föhringer Ring 6, D-80805, München, Germany.

Abstract

We take a new look at plaquette-plaquette correlators in 4d compact U(1) lattice gauge theory which are separated in time, both in the confined and the deconfined phases. From the behaviour of these correlators we extract glueball masses in the scalar as well as the axial-vector channels. Also in the deconfined phase, the non-zero momentum axial-vector correlator gives us information about the photon which appears as a massless particle in the spectrum. Using the Lüscher - Weisz multi-level algorithm, we are able to go to large time separations which were not possible previously.

I. INTRODUCTION

Compact U(1) lattice gauge theory in 4d exists in two phases separated by what is believed to be a weak first order transition. This theory does not have some complications of the non-Abelian gauge groups but still exhibits confinement of test charges in one of the phases due to the compact nature of its dynamical variables. Thus it is an ideal ground for testing various ideas relevant for confinement.

Abelian lattice gauge theory was first formulated and analyzed by Wilson in 1974 [1]. He concluded that at strong coupling the theory indeed confined static test quarks by looking at path ordered exponentials around closed paths (Wilson loops). A plausible mechanism of confinement was first given by Polyakov [2] who showed that in 3d confinement in Abelian lattice gauge theory could be thought of as due to the presence of a monopole plasma which produced an area law for the Wilson loop correlation function for all values of the coupling constant. The existence of monopoles even in a U(1) theory were a direct consequence of the compact nature of the dynamical variables. In 4d both Wilson and Polyakov conjectured

*e-mail:pushan@mppmu.mpg.de

†e-mail:ykoma@mppmu.mpg.de

‡e-mail:mkoma@mppmu.mpg.de

that there had to be a weakly coupled regime where test charges were not confined and thus the theory should have at least two distinct phases. The existence of a phase transition was finally proved by Guth [3].

Most of the analytical work was done in the “Villain approximation” where the original action is replaced by a quadratic action, but the periodicity of the variables is retained by using the Poisson summation formula. It was in this approximation that the existence of a massless photon was established in a weak coupling regime [4]. The Villain approximation achieves a separation between the perturbative and non-perturbative degrees of freedom. It is widely believed that the original action and the Villain action fall in the same universality class and therefore they should have the same critical behaviour. Except for the strong coupling limit, the model with its original action has mostly been studied numerically starting from [5].

Numerically practicable proposals to detect monopoles were first discussed by DeGrand and Toussiant [6] and now there is evidence that at strong coupling there is a non-zero monopole density (condensate) and beyond a certain coupling g_c the monopole density abruptly drops almost to zero. Therefore our present understanding is that compact U(1) lattice gauge theory exists in a confining and a deconfining phase which are separated by a phase transition. The confinement mechanism is thought to be due to the presence of monopoles and there are analogies to a dual superconductor mechanism [7]. In the deconfined phase, away from the transition region, one expects a massless photon. However nothing rigorous is known around the phase transition point.

Monte Carlo simulations have established that for the Wilson action the transition point corresponds to $\beta = 1.011128(11)$ [8]. The order of the transition has long been a matter of debate. Recent high statistics investigations including finite size scaling analysis have suggested a weak first order transition [8]. Other actions have also been studied and for the extended action which has two couplings, there have been interesting claims of the existence of a second order phase transition at particular values of these couplings [9].

Accurate measurements of the glueball mass can throw light on the order of the phase transition. However correlators in compact U(1) theory are difficult to handle numerically in the confining phase as the signal to noise ratio rapidly becomes worse with increasing distance. In fact except for points close to the phase transition [10] (where the glueball is lighter), such measurements have been carried out only for small temporal extents of the correlators [11].

Recently Lüscher and Weisz have proposed an exponential noise reduction method which exploits the local nature of the action and the existence of a positive definite transfer matrix [12]. Using this method, exponentially small values of Polyakov loop correlators at large separations have been measured reliably for both SU(2) [13] and SU(3) [14] gauge groups. Large Wilson loops have also been measured for SU(2) in 3d [13]. This gives the spectrum of the hadronic string. The breaking of the adjoint string [15], the 3-quark potential [16] and the glueball spectrum for SU(3) gauge group [17] have also been studied using this procedure. In this work we apply this error reduction procedure to 4d compact U(1) lattice gauge theory. We measure the scalar and axial vector glueball masses and also explore the masslessness of the photon close to the transition point in the deconfined phase.

The multi-level algorithm does not stipulate any fixed rule as how to measure a given observable and has to be applied differently in a way appropriate to the observable in ques-

tion. The methods we employ for the measurements are quite new and we believe are of as much importance as the results themselves. These methods let us go to large physical separations for the correlators in question. This is very important as at large separations, the contamination from higher excited states are small and the signals are relatively clean.

In section II we give the parameters of our simulation. Section III deals with the glueball correlators and there we explain how to use the multi-level algorithm to measure both scalar and the axial-vector glueball correlators. In section IV we present our results for the masses and in section V we present a discussion of our results.

II. SIMULATION DETAILS

In our simulations we use the Wilson action given by

$$S[U] = \beta \sum_{n,\mu,\nu} \{1 - \text{Re}(e^{i\theta_{\mu\nu}(n)})\}, \quad (1)$$

where $\theta_{\mu\nu}(n)$ is constructed from the dynamical variables $\theta_\mu(n)$ as

$$\theta_{\mu\nu}(n) = \theta_\mu(n) + \theta_\nu(n + \hat{\mu}) - \theta_\mu(n + \hat{\nu}) - \theta_\nu(n). \quad (2)$$

In this formulation $\theta_\mu(n)$ is compact and ranges $[-\pi, \pi]$. We impose periodic boundary conditions in all directions. The relation with continuum perturbation theory is obtained by identifying β with $1/g_0^2$, where g_0 is the bare coupling of the perturbation theory. All our simulations are done on a 16^4 lattice and on this lattice the phase transition occurs around $\beta = 1.0108$ [8]. We do not probe the transition too closely. The values of the coupling that we look at are given by $\beta = 0.990, 1.000, 1.005, 1.010$ in the confining region and $\beta = 1.012, 1.015$ and 1.020 in the deconfining region. To observe the photon we also simulate at $\beta = 1.03, 1.04, 1.05$ and 1.06 . We invoke the usual heatbath algorithm [18] and a ratio of one heatbath to three over-relaxations. We start from an ordered configuration (cold start) and use the first 1000 updates for thermalization.

To get an idea of the lattice spacing in the confining region, we use the string tension obtained from the Polyakov loop correlators [19]. Appealing to the universality of the string picture, we assume that in this case $\sqrt{\sigma}$ also corresponds to $(0.5 \text{ fm})^{-1}$. The string tension and the lattice spacings are then given by

β	0.99	1.0	1.005	1.01
$a^2\sigma$	0.231 (2)	0.164 (2)	0.123 (2)	0.063 (2)
$a(\text{fm})$	0.240 (1)	0.202 (2)	0.175 (2)	0.125 (2)

In the deconfined phase the string tension vanishes and we know that in the weak coupling limit the theory must go over to free electrodynamics which is a scale invariant theory. Therefore we do not attempt to set the scale in the deconfined regime.

III. GLUEBALL CORRELATORS

Glueballs in 4d compact U(1) lattice gauge theory were first investigated by Berg and Panagiotakopoulos [11]. They found that the masses in the scalar and the axial-vector channels with zero momentum fell quite sharply as one went towards the transition region from the confining phase but started rising again as one went towards the weak coupling region in the deconfined phase. In stark contrast masses from the momentum dependent axial-vector correlator dropped dramatically in the deconfined phase. Assuming the nearest neighbour lattice free field dispersion relation, they concluded that their data for the axial-vector correlator was consistent with the presence of a massless photon in this phase. These studies were carried out on a $4^3 \times 8$ lattice and consequently their lowest momentum was still quite high at $2\pi/4$. Glueball masses in U(1) were also looked at by Stack and Filipczyk [10]. They concluded that at least in the scalar channel, the glueball mass could be obtained by only looking at the monopole part of the Wilson loop. Glueball masses have also been studied extensively for the extended action [9]. However for that action the transition is expected to be of second order and therefore the critical behaviour is most likely quite different from the critical behaviour of the usual Wilson action.

A. Scalar channel

In this sub-section we explain how to measure glueball masses in the scalar channel using the multi-level scheme. To obtain the mass of this glueball, we measure the connected part of the correlator $\langle C(t)C(t_0) \rangle$ given by

$$\langle C(t)C(t_0) \rangle_{conn} = \left\langle \sum_{\mathbf{n}, i, j} P_{ij}(\mathbf{n}, t) \sum_{\mathbf{n}, i, j} P_{ij}(\mathbf{n}, t_0) \right\rangle - \left\langle \sum_{\mathbf{n}, i, j} P_{ij}(\mathbf{n}, t) \right\rangle \left\langle \sum_{\mathbf{n}, i, j} P_{ij}(\mathbf{n}, t_0) \right\rangle \quad (3)$$

where $P_{ij}(\mathbf{n}, t) = \exp(i\theta_{ij}(\mathbf{n}, t))$ is the plaquette in the ij plane. \mathbf{n} goes over all the points in a timeslice and i, j goes over the values 1, 2 and 3. This correlator is expected to behave like

$$\langle C(t)C(t_0) \rangle_{conn} \approx \alpha \left[e^{-m(t-t_0)} + e^{-m(N_t-(t-t_0))} \right], \quad (4)$$

where N_t is the extent of the lattice in the time direction. Fitting the measured correlator to this form, one can read off the mass m of the glueball. However this naive approach is not particularly suited for the multi-level algorithm.

One of the most efficient uses for the multi-level algorithm is to generate the small expectation values by multiplication rather than fine cancellation of positive and negative values of the same order. In equation (3) this advantage is lost since each expectation value is a number $\mathcal{O}(1)$, but the connected part is several orders of magnitude smaller than the full correlator. To get around this problem, we can take the derivative of the correlator to get rid of the vacuum expectation values of the plaquettes. So let us now take the derivative

of the correlator at both t and t_0 ¹ to obtain

$$\partial_t \partial_{t_0}^* \langle C(t) C(t_0) \rangle \approx \alpha \left[\partial_t e^{-mt} \partial_{t_0}^* e^{mt_0} + e^{-mNt} \partial_t e^{mt} \partial_{t_0}^* e^{-mt_0} \right]. \quad (5)$$

Taking ∂_t to be the forward derivative and $\partial_{t_0}^*$ to be the backward derivative on the lattice, we get,

$$\partial_t \partial_{t_0}^* \langle C(t) C(t_0) \rangle \approx -\alpha \left[e^{-m(t-t_0)} (1 - e^{-m})^2 + e^{-m(Nt-(t-t_0))} (e^m - 1)^2 \right]. \quad (6)$$

Now we are far better suited to apply the multi-level scheme. We can now measure

$$\partial_t \partial_{t_0}^* \langle C(t) C(t_0) \rangle = \left\langle \sum_{\mathbf{n}, i, j} [P_{ij}(\mathbf{n}, t+1) - P_{ij}(\mathbf{n}, t)] \sum_{\mathbf{n}, i, j} [P_{ij}(\mathbf{n}, t_0) - P_{ij}(\mathbf{n}, t_0 - 1)] \right\rangle, \quad (7)$$

where $[\dots]$ denotes the sub-lattice average of a quantity.

Sub-lattice averages, which were introduced in [12], are averages of quantities in their local environments. This requires partial updates of the lattice. In our case, for example, while estimating the expectation value of the plaquettes at time t (see fig. 1), the links in the spatial directions at time slices $(t+1)$ and $(t-1)$ are held fixed while the links between these fixed boundaries are updated using the usual mixture of heat-bath and over-relaxation. The sub-lattice averages are obtained by averaging the operator over these updated links. After several sub-lattice updates, the full lattice is updated as usual. The average over the sub-lattice updates constitutes one measurement in this case. Thus a measurement in the multi-level scheme is expensive, but the measured values are already quite stable and show very little fluctuation. This procedure uses crucially the locality of the action, as all the links which are affected by an updated link have to fit inside the slice of the lattice whose boundary is being held fixed during the update. The derivatives were estimated in the sub-lattice updates by taking the difference of the value of the operator on the updated slice with the value of the operator on the boundary. As shown in fig. 1, to get the forward derivative at t , we used the fixed boundary at $(t+1)$ and for the backward derivative, the boundary at $(t-1)$. To get the correlators one has to use two such slices (e.g. t and t_0 in fig. 1). In practice we hold every alternate layer of spatial links fixed and estimate the correlators for various time separations at the same time. The only drawback at the moment seems to be the fact that we have to consider a minimum separation of two in the temporal direction.

The number of sub-lattice updates is an optimization parameter of the algorithm that has to be tuned for efficient performance. This is a function of β . In the range of β we looked at, we found that 10 to 50 sub-lattice updates were sufficient. To compare this procedure with the naive algorithm we measured the percentage error on the correlators at a value of $(t-t_0)$ where both methods gave non-zero signals. In a similar amount of computer time, the multi-level algorithm produced errors which were about two orders of magnitude lower than the naive method.

¹In principle one derivative is enough, but in practice we found that the efficiency of the algorithm is higher for the double derivative compared to the single one.

FIGURES

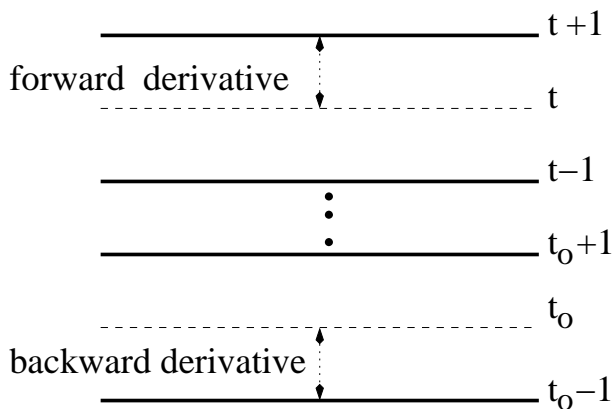


FIG. 1. Evaluation of the derivative of the glueball correlator. The thick lines are held fixed during the sub-lattice averaging.

B. Axial-vector channel

For glueball masses in the axial-vector channel, we follow the same procedure as in the scalar channel, except instead of the full plaquette, we now look at the correlation between the imaginary part of the space-like plaquettes separated by time Δt . In this channel, a zero momentum glueball is created by

$$B_{ij}(t) = \sum_{\mathbf{n}} \text{Im} P_{ij}(\mathbf{n}, t), \quad (8)$$

where again $P_{ij}(\mathbf{n}, t)$ is the plaquette in the ij plane, i and j go over 1, 2, 3 and \mathbf{n} goes over all the points in a time slice. This correlator does not have a vacuum expectation value. Therefore for this channel we do not have to take the derivatives before applying the multi-level scheme. We directly estimate

$$\langle [B_{ij}(t)][B_{ij}(t_0)] \rangle \approx \alpha [e^{-m_{\text{eff}}(t-t_0)} + e^{-m_{\text{eff}}(N_t-(t-t_0))}] \quad (9)$$

both in the confining as well as the deconfining phase.

The imaginary part of the plaquette is like $\sin(\theta_{ij})$ and under interchange of the indices ij , it picks up a negative sign. Thus $\sin(\theta_{ij})$ can be considered a 2-form. In the Hamiltonian formulation, the correlator of two 2-forms with momenta \mathbf{k} is given by

$$\begin{aligned} \langle B_{ij}(\mathbf{k}, t) B_{ij}(-\mathbf{k}, t_0) \rangle &= \int \prod_{\mathbf{n}} d\pi_i(\mathbf{n}) d\theta_i(\mathbf{n}) \\ &\times \left(\sum_{\mathbf{n}} \text{Im} e^{i\mathbf{k}\cdot\mathbf{n}} P_{ij}(\mathbf{n}, t) \right) \left(\sum_{\mathbf{n}} \text{Im} e^{-i\mathbf{k}\cdot\mathbf{n}} P_{ij}(\mathbf{n}, t_0) \right) e^{-\beta\mathcal{H}(\theta, \pi)} \quad (10) \end{aligned}$$

where θ_i are the dynamical variables and π_i the canonically conjugate momenta. Each component of \mathbf{k} takes the values $2\pi l/N_s$ where N_s is the spatial extent of the lattice and l

is an integer going from 1 to N_s . If d is the exterior derivative, then, as in the continuum, $d^2 = 0$ also holds on the lattice [20] and we can rewrite B as $dA + H$ where A is a 1-form and H is the part of B that cannot be written as d of a 1-form. Inserting this decomposed version into Eq.(10) we get

$$\langle B_{ij}B_{ij} \rangle \approx Tr \left(\sum_{\mathbf{n}} e^{i\mathbf{k}\cdot\mathbf{n}} (\partial_{[i}A_{j]} + H_{ij}) \right) e^{-m_{\text{eff}}(t-t_0)} \left(\sum_{\mathbf{n}} e^{-i\mathbf{k}\cdot\mathbf{n}} (\partial_{[i}A_{j]} + H_{ij}) \right), \quad (11)$$

where we have assumed that states of a definite momentum, which are eigenstates of B by construction also diagonalise the Hamiltonian \mathcal{H} . This is certainly true in the weak coupling region, but we believe, is not a bad approximation to make throughout the deconfined phase. Next doing an integration by parts and recalling that we have periodic boundary conditions, we get

$$\langle B_{ij}B_{ij} \rangle \approx Tr \left(\sum_{\mathbf{n}} A_j k_i + \sum_{\mathbf{n}} e^{i\mathbf{k}\cdot\mathbf{n}} H_{ij} \right) \left(\sum_{\mathbf{n}} A_j k_i + \sum_{\mathbf{n}} e^{-i\mathbf{k}\cdot\mathbf{n}} H_{ij} \right) e^{-m_{\text{eff}}(t-t_0)}. \quad (12)$$

Thus the correlator has a momentum dependent part which is sensitive to a correlator between two 1-forms. In the deconfining region we expect this part to yield information about the photon which we know exists in the weak coupling regime. It is interesting to observe that at $\mathbf{k} = 0$ there is no photon contribution to the $\langle BB \rangle$ correlator Eq.(10), hence one has to consider a non-zero total momentum to see the photon.

IV. RESULTS

A. Scalar channel

In the scalar channel we measured both $\partial_t \partial_{t_0}^* \langle C(t)C(t_0) \rangle$ and $\partial_t^* \partial_{t_0} \langle C(t)C(t_0) \rangle$. The only difference between the two quantities is the interchange of coefficients $(1 - e^{-m})^2$ and $(e^m - 1)^2$. As can be easily seen from the explicit form given in Eq. (6), both the functions can be rewritten as $\Gamma' \cosh(m\Delta t)$. We folded the data about the symmetry point and performed correlated fits to this form over different ranges of Δt . The effective masses and χ^2 from the fits are given in table I.

The effective masses obtained from the two sets are consistent with each other within error bars. We also see that at the smallest value of Δt , the effective masses have significant contamination from the higher states. This effect becomes more and more pronounced as one approaches the phase transition. In fig. 2 we plot the correlation functions themselves.

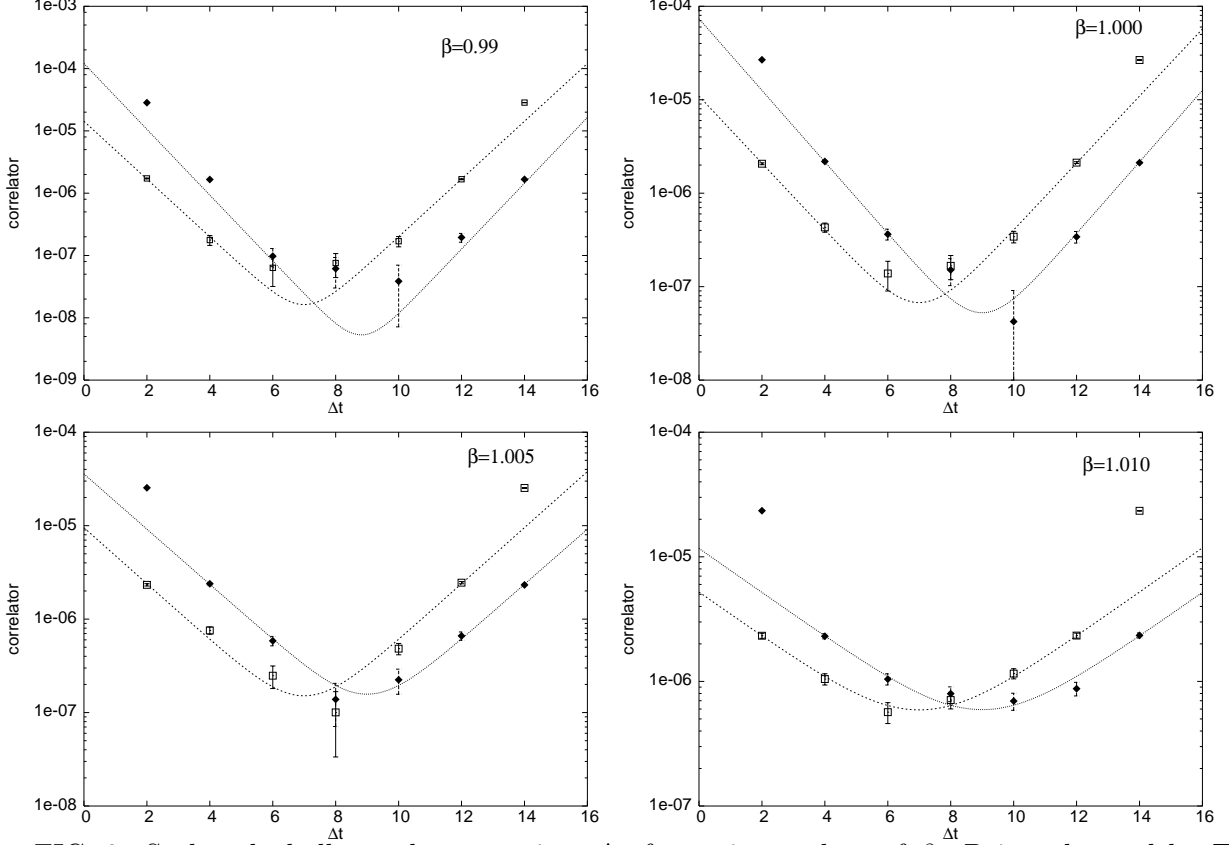


FIG. 2. Scalar glueball correlators against Δt for various values of β . Points denoted by \square come from $\partial_t \partial_{t_0}^* \langle C(t)C(t_0) \rangle$ while the ones denoted by \blacklozenge come from $\partial_t^* \partial_{t_0} \langle C(t)C(t_0) \rangle$.

In these figures, points denoted by square (\square) come from the correlator $\partial_t \partial_{t_0}^* \langle C(t)C(t_0) \rangle$ while the ones denoted by the filled diamond (\blacklozenge) come from the set $\partial_t^* \partial_{t_0} \langle C(t)C(t_0) \rangle$. At $\beta = 1.000$ and 1.010 , where we could compare, our data is completely consistent with the values reported in [10,11].

Finally we plot the masses we have obtained from our simulations along with the prediction from the strong coupling expansion in fig. 3. The strong coupling expansion for the scalar glueball mass is [21]

$$m = -4 \log u + \sum_{k=1}^{\infty} m_k u^k \quad (13)$$

where u is given by $u = I_1(\beta)/I_0(\beta)$ for the group $U(1)$ and the coefficients m_k till the eighth order are $m_2 = \frac{3}{2}$, $m_4 = -\frac{793}{24}$, $m_6 = -\frac{1783}{24}$ and $m_8 = -\frac{1660309}{2880}$. The coefficients of the odd powers of k are zero upto this order. From this figure we see that either the simulation points lie outside the radius of convergence of the strong coupling expansion or the higher order coefficients come with different signs.

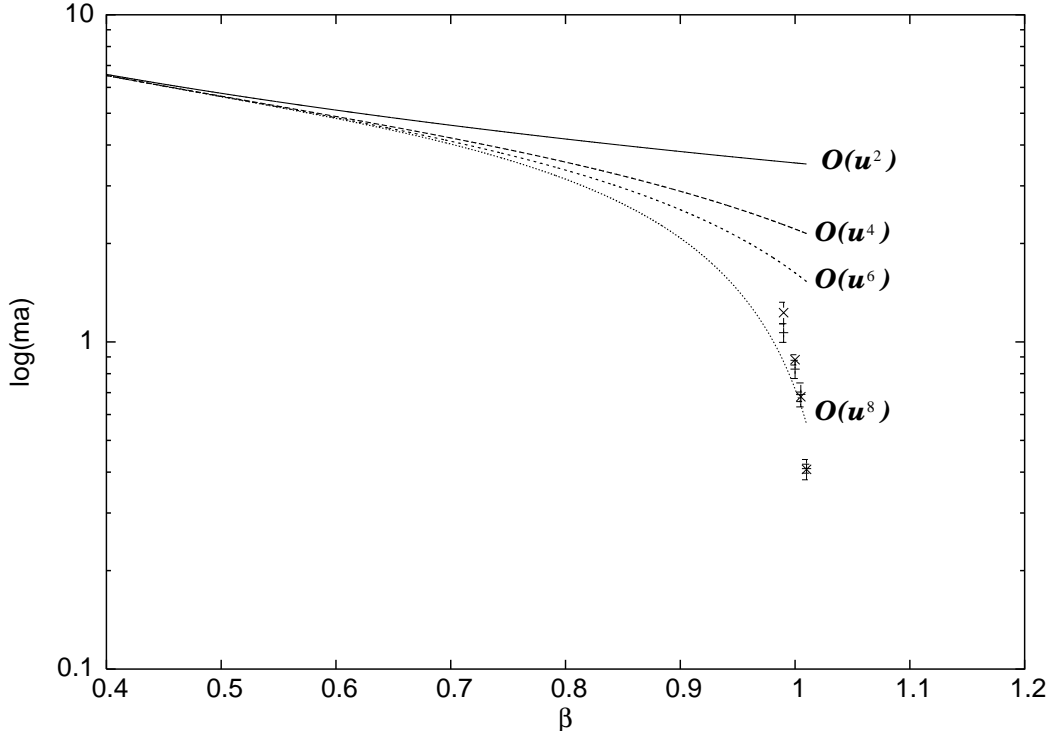


FIG. 3. Scalar glueball masses and the strong coupling expansions.

B. Axial vector channel

In the axial vector channel, we construct states with zero as well as with definite momenta. The explicit form of the correlator is given in Eq.(9). To obtain the effective masses from the correlators, we again fold the data about the symmetry point ($\Delta t = 8$ in this case) and perform a correlated fit to

$$f(\Delta t) = A \cosh(m_{\text{eff}} \Delta t). \quad (14)$$

In table II we present the effective masses from the axial-vector correlators along with the range of the fit, the momenta and the correlated χ^2 as obtained from the fits. In fig. 4 we plot the zero momentum correlators at β values 1.000 (\blacktriangle), 1.005 (\blacksquare) and 1.010 (\blacktriangledown).

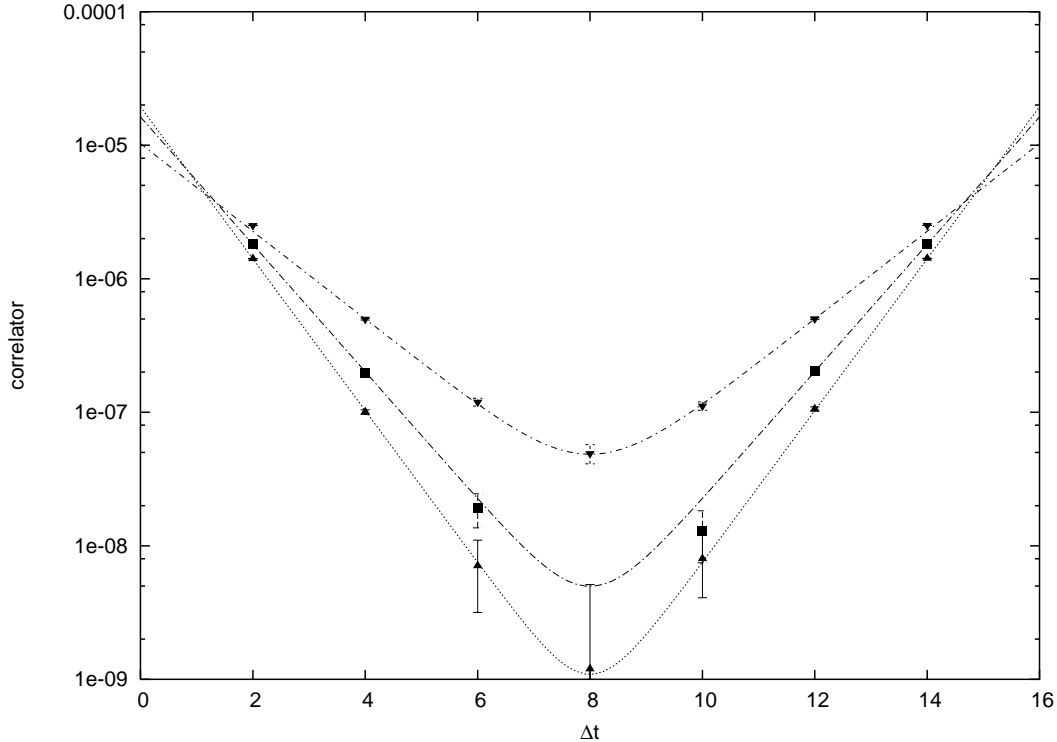


FIG. 4. Axial-vector correlators with zero momentum against Δt . $\beta = 1.000$ (\blacktriangle), 1.005 (\blacksquare) and 1.010 (\blacktriangledown)

V. DISCUSSION

In section III we have seen that the momentum dependent axial vector correlator is sensitive to the photon in the deconfined region. However to extract a massless particle we need to subtract the momentum contribution to the effective mass and therefore specify the dispersion relation for this particle. As a first approximation we assume that the particle obeys the lattice free field dispersion relation [11]

$$m_{\text{eff}}^2 = m_{\text{rest}}^2 + \sum_{i=1}^3 (2 - 2 \cos k_i), \quad (15)$$

and check whether this assumption is consistent with our data or not.

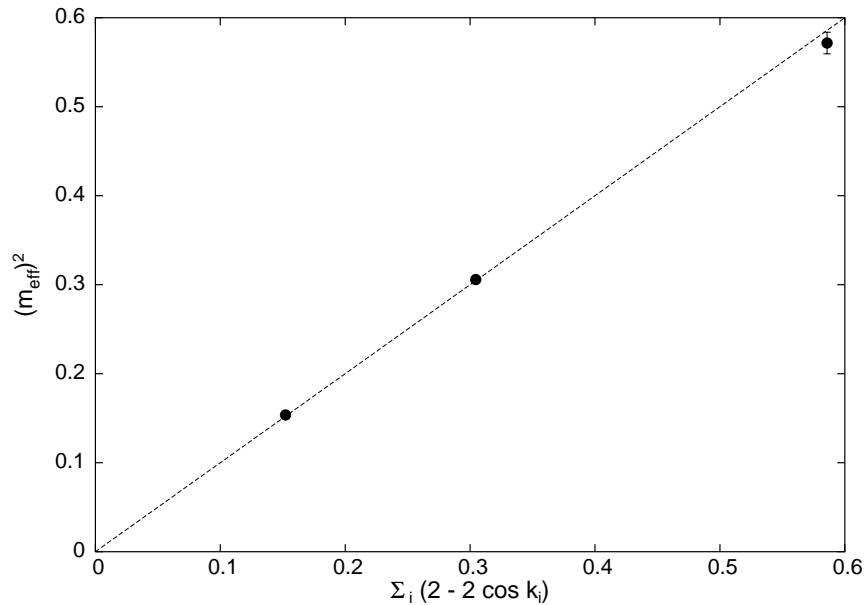


FIG. 5. Consistency of the free field dispersion relation Eq.(15) with the effective masses from the axial-vector correlator at $\beta = 1.015$. The momentum contribution to m_{eff} due to (k_x, k_y, k_z) are plotted along the x -axis.

In fig. 5, the filled circle (\bullet) denotes the effective masses at $\beta = 1.015$ for the momenta $(k_x, k_y, k_z) = (2\pi/16, 0, 0), (2\pi/16, 2\pi/16, 0)$ and $(4\pi/16, 0, 0)$. The x -axis is the contribution to m_{eff} due to these momenta, assuming the lattice free field dispersion relation. The values used in this plot are given in table II along with the effective masses. We have used values over the smaller range of Δt (4 - 8) as that had a much lower $\chi^2/d.o.f$. From the plot it is clear that within our statistical error bars, the data is completely consistent with a massless particle obeying the free field dispersion relation. While there is no justification to assume that this simplest relation holds close to the phase transition point, our data shows that any deviation would have to be small.

To see the behaviour of this massless particle at various values of β , we have plotted the effective masses obtained from the momentum dependent axial-vector correlators in fig. 6. Here the triangles (Δ) correspond to effective masses obtained by fitting over the whole range of Δt while the inverted triangles (∇) are the masses obtained by dropping the smallest value of Δt . The filled circle (\bullet) has been obtained by subtracting the momentum contribution from the inverted triangles assuming free field dispersion relation and the dotted lines are the 3σ bands for this set. The actual values along with the 1, 2 and 3σ limits are given in table III.

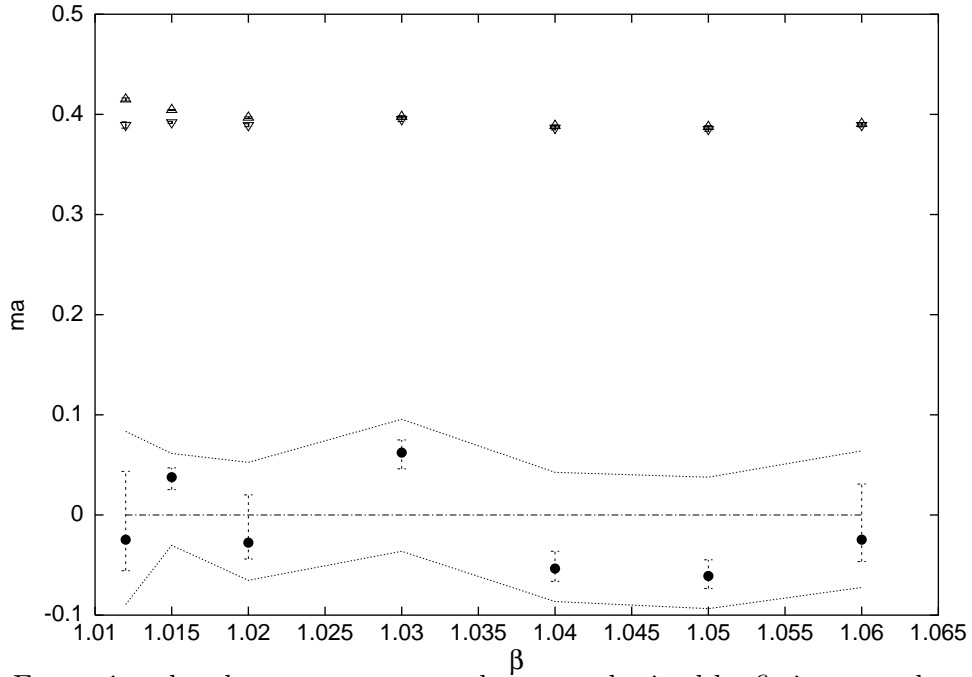


FIG. 6. Extracting the photon. Δ correspond to m_{eff} obtained by fitting over the whole range of Δt while ∇ are m_{eff} obtained by dropping the smallest value of Δt . \bullet has been obtained by removing the momentum contribution assuming Eq.(15) and the dotted lines are the 3σ bands for this set. (Note that the zero-momentum correlator has no contribution from the photon. The dominant contribution comes from the correlator with the lowest possible non-zero momenta on the lattice.)

From this figure it is clear that we are sensitive to the presence of higher states up to $\beta = 1.02$. Beyond this, dropping the smaller values of Δt do not yield significantly different values of the effective mass. Moreover within statistical fluctuations all the masses are consistent with zero.

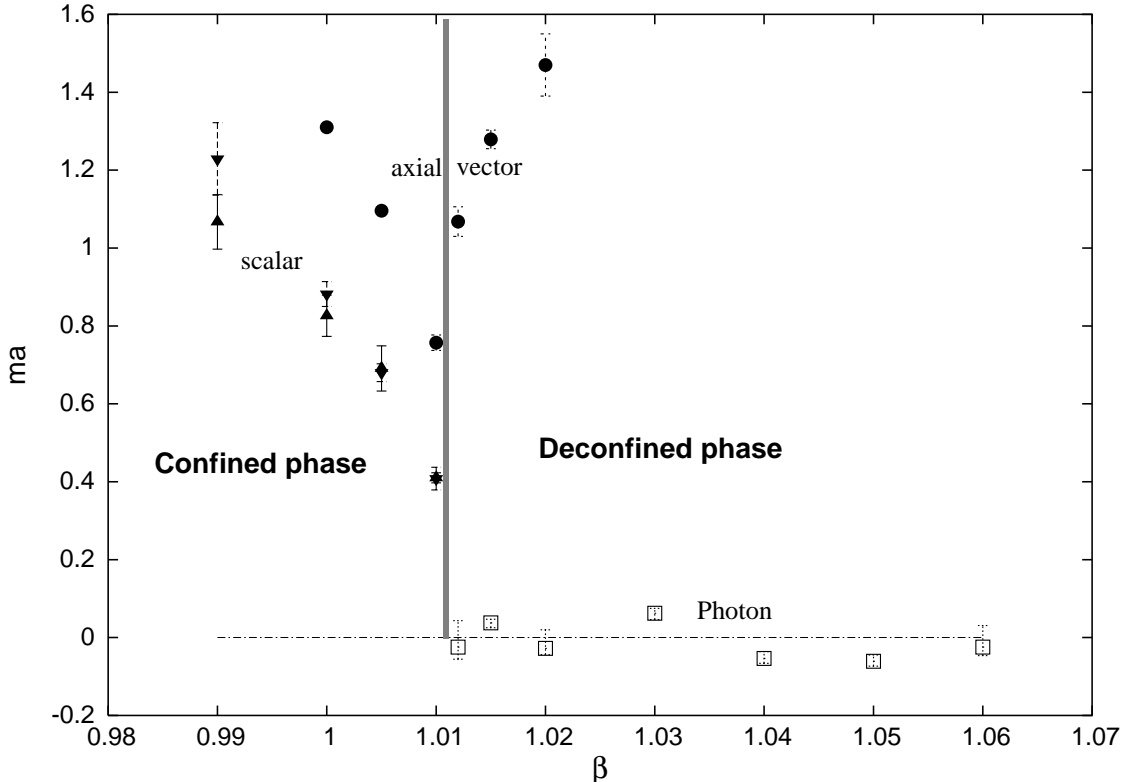


FIG. 7. Consolidated plot of glueball masses. \blacktriangle and \blacktriangledown are the scalar glueball masses from the sets $\partial\partial^*\langle CC\rangle$ and $\partial^*\partial\langle CC\rangle$ respectively. The \bullet corresponds to the axial vector mass with zero momentum. The \square is the photon extracted from the axial vector correlator (See fig. 6).

Finally in fig. 7, we plot the masses from all the channels along with the region where the phase transition is believed to take place. The filled triangle (\blacktriangle) and the filled inverted triangle (\blacktriangledown) are the scalar glueball masses from the sets $\partial\partial^*\langle CC\rangle$ and $\partial^*\partial\langle CC\rangle$ respectively. The filled circle (\bullet) corresponds to the axial vector mass where the momentum has been set to zero. The square (\square) is the photon extracted from the axial vector correlator (fig. 6). From this figure we see that on the confining side the scalar mass falls to about 0.41 in lattice units near the phase transition while the axial vector mass at 0.76 lattice units is nearly twice that value. However none of them seem to go to zero. Although we have not done a finite size analysis, our lattice volume itself is reasonably large : $(\sim 2fm)^4$ near the phase transition. Also during equilibration at $\beta = 1.010$ we observed that the plaquette seemed to get stuck in a different phase for some time when we started from an ordered configuration. Putting these two facts together we believe that our data points towards a first order phase transition which is in agreement with [8]. In the deconfined region we see a remarkable difference between the zero momentum and the non-zero momentum correlators. While the zero momentum correlators vary over two orders of magnitude as the Δt varies, the correlators with definite momenta hardly seem to change. In fact if we subtract the free field momentum dependence we get rest masses which are zero within errors. We believe this is numerical evidence for the photon in the deconfined phase.

The final picture that emerges from our study is that the general scenario presented in [11] does not change. The momentum dependent correlator indeed seems to indicate the

presence of a zero mass particle in the deconfined phase and the axial vector which comes from the zero momentum part seems to get heavy and decouple from the theory. We have carried out the analysis on a 16^4 lattice and have obtained the masses from correlators which are separated by 2 to 8 lattice spacings. This lets us disentangle the effect of the higher states to the effective masses of the lightest glueballs and therefore yields much more accurate results. In spite of such large temporal separations ($\sim 1fm$ in terms of our scale), the multi-level scheme of measurements together with taking the derivatives to get rid of the non-zero vacuum expectation values, allow us to obtain accurate data. This demonstrates the power of this method which should be applicable in the non-Abelian cases as well.

Our study also helps further consolidate the pattern of glueball masses in U(1) lattice gauge theory and points towards a first order confinement deconfinement phase transition. Furthermore we present strong evidence for a massless photon in the deconfined phase of the theory.

VI. ACKNOWLEDGEMENTS

The authors would like to express their gratitude to Peter Weisz and Erhard Seiler for constant encouragement and numerous discussions during the course of this work. We are also indebted to Martin Lüscher for suggesting the use of derivatives and to Tom DeGrand for several useful comments and help with the correlated fitting. Thanks are also due to Pierre Van Baal and Ferenc Niedermayer for a critical reading of the manuscript and several useful suggestions.

Finally PM would like to thank the Rechen Zentrum Garching and the Max-Planck-Institut for the computing facilities and YK and MK would like to thank SX5 at RCNP, Osaka University where part of the computation was carried out.

REFERENCES

- [1] K. G. Wilson, Phys. Rev. D10 (1974) 2445
- [2] A. M. Polyakov, Phys. Lett. B59 (1975) 82
- [3] A. H. Guth, Phys. Rev. D21 (1980) 2291
- [4] J. Fröhlich, T. Spencer, Comm. Math. Phys. 83 (1982) 411
- [5] M. Creutz, L. Jacobs, C. Rebbi, Phys. Rev. D20 (1979) 1915
- [6] T.A. DeGrand, D. Toussaint, Phys. Rev. D22 (1980) 2478
- [7] T. Banks, R. Myerson, J. B. Kogut, Nucl. Phys. B129 (1977) 493 Michael E. Peskin, Annals Phys. 113 (1978) 122
- [8] G. Arnold, T. Lippert, K. Schilling, T. Neuhaus, Nucl. Phys. Proc. Suppl. 94, (2001) 651, hep-lat/0011058.
- [9] J. Jersak, T. Neuhaus, H. Pfeiffer, Phys. Rev. D60 (1999) 054502, hep-lat/9903034; J. Cox, J. Jersak, H. Pfeiffer, T. Neuhaus, P.W. Stephenson, A. Seyfried, Nucl. Phys. B545 (1999) 607, hep-lat/9808049; J. Cox, W. Franzki, J. Jersak, C.B. Lang, T. Neuhaus, P.W. Stephenson, Nucl. Phys. B499 (1997) 371, hep-lat/9701005
- [10] J.D. Stack, R. Filipczyk, Nucl. Phys. Proc. Suppl. 63 (1998) 537
- [11] B. Berg, C. Panagiotakopoulos, Phys. Rev. Lett. 52 (1984) 94
- [12] M. Lüscher, P. Weisz, JHEP 0109 (2001) 010, hep-lat/0108014.
- [13] P. Majumdar, Nucl. Phys. B664 (2003) 213, hep-lat/0211038.
- [14] M. Lüscher, P. Weisz, JHEP 0207 (2002) 049, hep-lat/0207003.
- [15] S. Kratochvila and P. de Forcrand, Contribution to 20th International Symposium on Lattice Field Theory, hep-lat/0209094.
- [16] C. Alexandrou, P. de Forcrand and O. Jahn, Contribution to 20th International Symposium on Lattice Field Theory, hep-lat/0209062.
- [17] H. B. Meyer, JHEP 0301 (2003) 048, hep-lat/0209145
- [18] M. Lüscher, Simulation Program for the pure U(1) gauge theory.
- [19] Y. Koma, M. Koma, P. Majumdar (In preparation).
- [20] M. Lüscher, Nucl. Phys. B538 (1999) 515
- [21] G. Münster, Nucl. Phys. B256 (1985) 67

TABLES

β	range of Δt	$\partial_t^* \partial_{t_0} \langle C(t)C(t_0) \rangle$		$\partial_t \partial_{t_0}^* \langle C(t)C(t_0) \rangle$	
		m	$\chi^2/d.o.f$	m	$\chi^2/d.o.f$
0.990	2 - 8	1.414 (7)	8.8/2	1.402 (7)	21.51/2
	4 - 8	1.195 (55)	2.8/1	1.085 (50)	4.04/1
1.000	2 - 8	1.241 (8)	38.01/2	1.2485 (80)	60.73/2
	4 - 8	0.875 (41)	0.53/1	0.812 (37)	3.219/1
1.005	2 - 8	1.1545 (90)	93.06/2	1.1455 (90)	88.64/2
	4 - 8	0.682 (29)	0.11/1	0.693 (29)	0.127/1
1.010	2 - 8	1.075 (15)	215.7/2	1.065 (14)	227.8/2
	4 - 8	0.405 (22)	4.26/1	0.410 (21)	0.0039/1

TABLE I. Scalar glueball masses

β	momenta	range of Δt	m_{eff}	$\chi^2/d.o.f.$
1.000	(0,0,0)	2 - 8	1.31 (1)	0.0013/2
1.005	(0,0,0)	2 - 6	1.096 (9)	3/1
1.010	(0,0,0)	2 - 8	0.809 (5)	5.31/2
		4 - 8	0.757 (20)	0.012/1
1.012	(0,0,0)	1 - 3	1.068 (38)	2.26/1
	(2 π /16,0,0)	2 - 8	0.4149 (16)	80.0/2
		4 - 8	0.3894 (32)	0.36/1
1.015	(0,0,0)	2 - 8	1.278 (24)	5.7/2
		2 - 6	1.279 (24)	0.24/1
	(2 π /16,0,0)	2 - 8	0.4044 (5)	256.0/2
		4 - 8	0.3920 (10)	3.43/1
	(2 π /16,2 π /16,0)	2 - 8	0.5685 (10)	31.84/2
		4 - 8	0.553 (3)	0.022/1
	(4 π /16,0,0)	2 - 8	0.766 (2)	1.59/2
		4 - 8	0.756 (8)	0.0069/1
1.020	(0,0,0)	2 - 8	1.47 (8)	0.46/2
	(2 π /16,0,0)	2 - 8	0.3968 (8)	30.82/2
		4 - 8	0.3892 (15)	0.39/1
1.030	(2 π /16,0,0)	2 - 8	0.3976 (11)	3.06/2
		4 - 8	0.3951 (22)	1.4/1
1.040	(2 π /16,0,0)	2 - 8	0.3885 (10)	1.87/2
		4 - 8	0.3865 (20)	0.61/1
1.050	(2 π /16,0,0)	2 - 8	0.3875 (12)	6.4/2
		4 - 8	0.3854 (22)	5.2/1
1.060	(2 π /16,0,0)	2 - 8	0.3905 (10)	0.36/2
		4 - 8	0.3894 (20)	0.03/1

TABLE II. Mass from the axial-vector correlator.

β	m_{eff}	m_{rest}	1 σ limits		2 σ limits		3 σ limits	
1.012	0.3894 (32)	-0.0247	-0.0556	0.0435	-0.0745	0.0665	-0.0894	0.0834
1.015	0.3920 (10)	0.0377	0.0253	0.0470	-0.0119	0.0547	-0.0303	0.0615
1.020	0.3892 (15)	-0.0276	-0.0439	0.0201	-0.0556	0.0397	-0.0652	0.0525
1.030	0.3951 (22)	0.0622	0.0461	0.0749	0.0201	0.0858	-0.0362	0.0955
1.040	0.3865 (20)	-0.0535	-0.0663	-0.0362	-0.0770	0.0158	-0.0864	0.0426
1.050	0.3854 (22)	-0.0609	-0.0735	-0.0448	-0.0841	-0.0172	-0.0935	0.0377
1.060	0.3894 (20)	-0.0247	-0.0465	0.0309	-0.0609	0.0502	-0.0724	0.0640

TABLE III. Level of significance of nonzero m_{rest} for the photon.